Measurements of diffractive processes at HERA

Aharon Levy
Tel Aviv University, Tel Aviv, Israel
for the H1 and ZEUS Collaborations

1 Introduction

One of the main objectives in ep interactions is to study the structure of the proton. This is done by performing a deep inelastic scattering (DIS) process in which the virtual photon probes the partonic structure of the proton. All events are studied, like in a total cross section experiment.

If, however, the final state consists of events in which the proton remains intact, or there is a large rapidity gap (LRG), we have diffractive events, mediated by a color singlet exchange. These can be further classified as inclusive diffractive events, as depicted in Fig. 1, or as exclusive ones, shown in Fig. 2. In this talk, these two classes of processes will be studied.

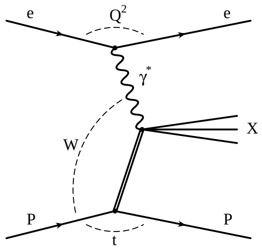

Fig. 1. Schematic diagram for inclusive diffractive DIS ep reaction.

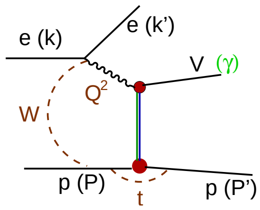

Fig. 2. Schematic diagram for exclusive diffractive electroproduction of vector mesons V.

The color singlet exchange is presented in the Regge theory of strong interactions [1] as the soft Pomeron, introduced by Gribov [2], and the parameters of its trajectory have been determined by Donnachie and Landshoff [3]. In contrast to the universal nature of this exchange, in the language of Quantum Chromodynamics (QCD), the color singlet exchange is described as a two gluon exchange [4]. Since its properties depend on the scale involved in the interaction, the QCD Pomeron has a non-universal character. We will discuss the results with respect to the soft and the hard behavior of these two approaches, which manifests themselves in the energy behavior of the cross sections.

2 Kinematics of diffractive scattering

The variables used in diffractive scattering can be defined using the four vectors presented in Fig. 3. The usual DIS variables are the negative of the mass squared of the virtual photon, $Q^2 = -q^2 = -(k-k')^2$, the square of the center of mass energy of the $\gamma^* p$ system, $W^2 = (q+p)^2$, the Bjorken scaling variable, $x = \frac{Q^2}{2p \cdot q}$, which in the Quark Parton Model can be thought of as the fraction of the proton momentum carried by the interacting quark, and the inelasticity, $y = \frac{q \cdot p}{k \cdot p}$.

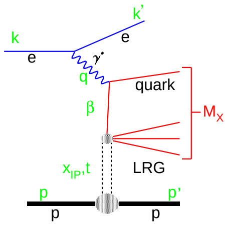

Fig. 3. Schematic diagram of diffractive ep interaction.

In addition to the above variables, the variables used to describe the diffractive final state are

$$
\begin{aligned}
x_{I\!P} &= \frac{q \cdot (p-p')}{q \cdot p} \simeq \frac{Q^2 + M_X^2}{Q^2 + W^2} \\
\beta &= \frac{Q^2}{2q \cdot (p-p')} \simeq \frac{Q^2}{Q^2 + M_X^2} \\
t &= (p-p')^2 .
\end{aligned}
$$

The fractional proton momentum which participates in the interaction with γ^* is $x_{I\!P}$, and β is the equivalent of Bjorken x but relative to the exchanged object. M_X is the invariant mass of the hadronic final state recoiling against the leading proton, $M_X^2 = (q+p-p')^2$. The approximate relations hold for small t and large W.

3 Diffraction as soft or hard process

In the Regge description, diffraction is a soft process. Its properties are determined by the universal Pomeron trajectory, $\alpha_{I\!P}(t) = \alpha_{I\!P}(0) + \alpha'_{I\!P} t$, with $\alpha_{I\!P}(0) = 1.081$ and $\alpha'_{I\!P} = 0.25$ GeV^{-2}. Therefore the energy behavior of the total $\gamma^* p$ cross section is expected to be $\sigma_{tot} \sim (W^2)^{\alpha_{I\!P}(0)-1} \simeq W^{0.16}$. Both the elastic and the inclusive diffraction cross section are expected to have a faster rise with energy $\sim (W^2)^{2\alpha_{I\!P}(0)-2}/b$, where b is the slope of the differential cross section in t [5].

In the perturbative QCD picture, the diffractive process is viewed, in the proton rest frame, as follows: the virtual photon fluctuates into a quark-antiquark pair, which interact diffractively with the proton by exchanging two gluons. Therefore, in this case, the diffractive cross section is proportional to the square of the gluon density. Since the gluon density, $xg(x, Q^2) \sim x^{-\lambda} \sim (W^2)^{\lambda}$, where λ depends on the scale Q^2, the diffractive cross section has an energy behavior $\sim (W^4)^{\lambda(Q^2)}$. At $Q^2 = 10$ GeV^2, for example, $\lambda \approx 0.2$, and thus the cross section would have a $W^{0.8}$ dependence.

The above discussion shows that we expect a transition from soft to hard processes when the virtuality of the probing photon increases.

4 Inclusive diffraction

One can express the inclusive cross section by a diffractive structure function F_2^D which is a function of four variables, $x_{I\!P}, t, x, Q^2$. It was shown [6–8] that QCD factorization holds also in case of diffraction. Thus F_2^D can be decomposed into diffractive parton distributions, which would follow the same DGLAP evolution equation that apply in the DIS inclusive case. If, in addition, one postulates Regge factorization, in the spirit of Ingelman and Schlein [9], F_2^D may be decomposed into a universal $I\!P$ flux and the structure function of the $I\!P$. One usually integrates over the t variable, and this decomposition is written as

$$\frac{dF_2^{D(3)}(x, Q^2, x_{I\!P})}{dx_{I\!P}} = f_{I\!P}(x_{I\!P}) F_2^{I\!P}(\beta, Q^2),$$

where the $x_{I\!P}$ dependence of the flux is universal, independent of β and Q^2 and is given by $f_{I\!P}(x_{I\!P}) \sim x_{I\!P}^{1-2\alpha_{I\!P}(0)}$.

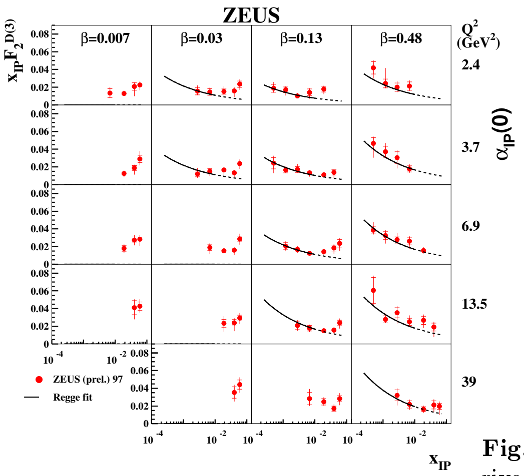

Fig. 4. $x_{I\!P}$ dependence of $x_{I\!P} F_2^{D(3)}$ at fixed β and Q^2 values, as denoted in the figure.

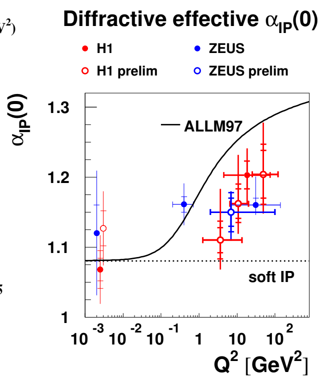

Fig. 5. Q^2 dependence of $\alpha_{I\!P}(0)$ derived from measurements of diffractive and total $\gamma^* p$ cross sections. The curve (ALLM97) is a representation of the results obtained in inclusive DIS measurements.

An example [10] of the $x_{I\!P}$ dependence of $x_{I\!P} F_2^{D(3)}$ at fixed β and Q^2 values, is shown in Fig. 4. The curves are the best fit to the data (restricted to $x_{I\!P} < 0.01$) using a universal flux, as described above, with $\alpha_{I\!P} = 1.16 \pm .01(\mathrm{stat})^{+.04}_{-.01}(\mathrm{syst})$. This value, together with a compilation from other measurements [11], is displayed in Fig. 5. For comparison, also shown is the Q^2 dependence of $\alpha_{I\!P}(0)$ derived from the inclusive DIS measurements and conveniently represented by the ALLM97 parameterization [12]. Clearly, the inclusive DIS data are not compatible with a universal $I\!P$ trajectory. The diffractive measurements seem to point to some Q^2 dependence, though the uncertainties are too large for a firm conclusion. For $Q^2 > 10$ GeV^2, the value of $\alpha_{I\!P}(0)$ is significantly higher than that expected from the soft Pomeron.

The β and Q^2 dependence of the Pomeron structure function, as measured by the H1 collaboration [11], are shown in Fig. 6. It is the Pomeron structure function under the assumption that the longitudinal diffractive structure function is zero, $F_L^D = 0$, and that Regge factorization holds, and therefore one divides-out the Pomeron flux. One sees that, just like in the inclusive DIS case, as Q^2 increases, the Pomeron structure function is consistent with a rising behavior towards low β. However, unlike the inclusive DIS case, positive scaling violations are observed up to large β values, and only for $\beta >$ 0.8, the scaling violations turn negative.

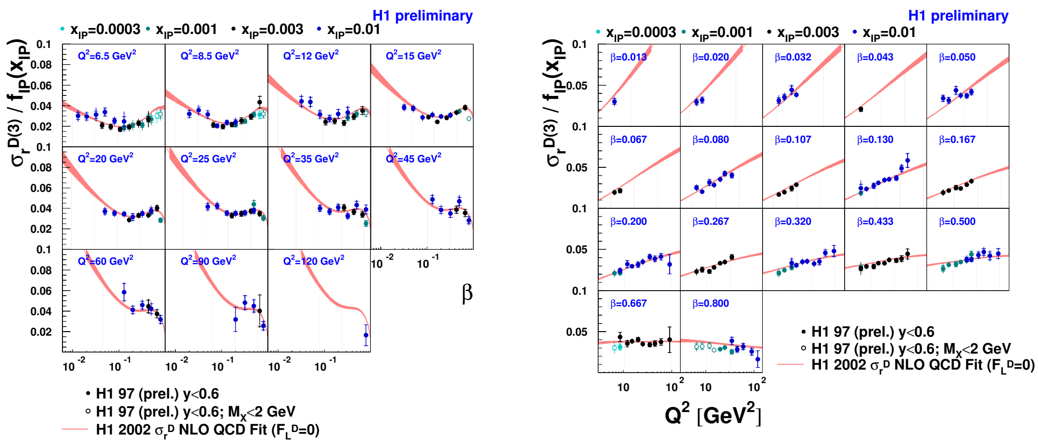

Fig. 6. The Pomeron structure function dependence on β (left) and on Q^2 (right). The curves are a result of a NLO QCD fit, assuming $F_L^D = 0$.

A NLO QCD fit, assuming $F_L^D = 0$, was performed to the data and a good description of the data is obtained. The resulting parton density distributions in the Pomeron are shown in Fig. 7. They do not differ much from a LO QCD fit, and have the feature of a sizable contribution of the gluon density at large z (which is same as β). Using the parton densities from the NLO fit, one gets a good description of the β and $x_{I\!P}$ distribution of diffractive jet production [13] and diffractive D^* production [14].

One can calculate the momentum fraction taken by the gluons. This turns out to be a large fraction, about 0.75 ± 0.15 at $Q^2 = 10$ GeV^2, and almost Q^2 independent, as can be seen in Fig. 8. Frankfurt and Strikman [15] used this to calculate the probability that a gluon from the proton will produce a diffractive process. They find that at $x = 10^{-3}$ and $Q^2 = 4$ GeV^2, this probability is as high as 0.4, which is very close to the unitarity limit of 0.5.

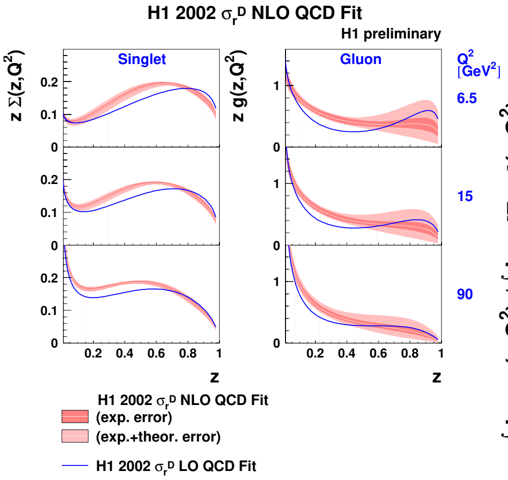

Fig. 7. The resulting parton density distributions in the Pomeron, using a NLO QCD fit (shaded line) compared to a LO fit (solid line).

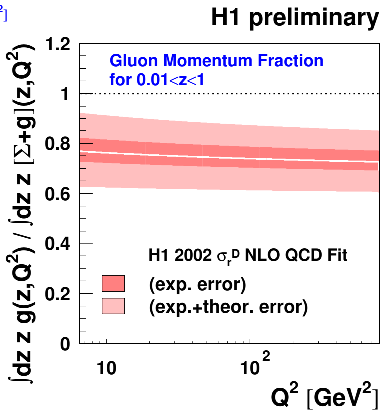

Fig. 8. The gluon momentum fraction from a NLO QCD fit, as function of Q^2.

The ratio of the diffractive cross section to the total $\gamma^* p$ cross section is shown in Fig. 9, as function of Q^2, for fixed β values. This ratio, is remarkably flat over a wide kinematic range. The ratio is flat also as function of W for fixed M_X values [16], contrary to expectations from Regge phenomenology.

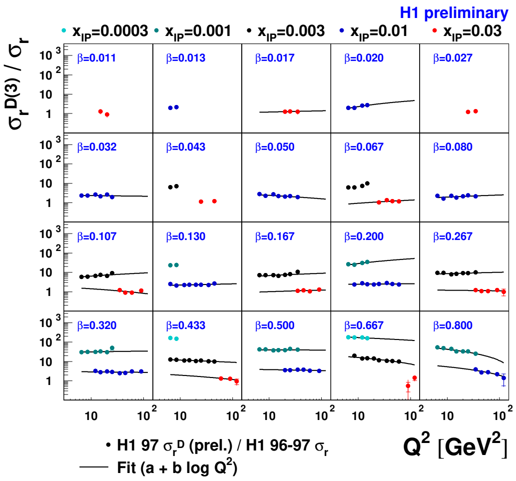

Fig. 9. The ratio of the diffractive to total cross section as function of Q^2, for fixed β values.

5 Exclusive Vector Mesons

It has been suggested [17] that a good way to see more clearly the different behavior of soft and hard processes is to study diffractive production of low masses, in particular vector mesons. Exclusive vector meson (VM) production show a clear interplay between soft and hard diffractive processes. One of the nice examples to this effect can be seen in case of the elastic photoproduction of VMs, whose cross section measurements as function of W are presented in Fig. 10. There is a clear change in the W dependence when going from the light VMs, like ρ^0, ω and ϕ, to the heavier ones like $J/\psi, \psi(2S)$ and Υ. In the latter case, a hard scale is provided by the mass of the heavy quarks. The shallower W dependence of the light VMs is consistent with that expected from a soft process, mediated by the $I\!P$ trajectory, while the steep W dependence in case of the heavy VMs is consistent with expectations from a two-gluon exchange hard diffractive process calculated in pQCD.

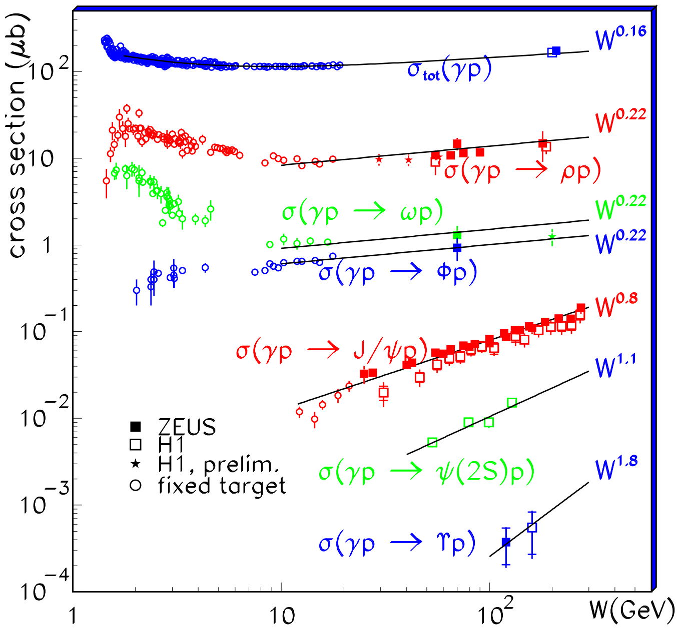

Fig. 10. Compilation of elastic photoproduction of vector mesons, as function of W. The total γp cross section is plotted for comparison.

Another soft-hard transition can be obtained by using Q^2 as a scale in case of exclusive electroproduction of ρ^0 [18,19]. This is demonstrated in Fig. 11, where the δ parameter, of the W^δ behavior of the cross section, is plotted as function of Q^2. While at low Q^2, δ is consistent with expectations of a soft process, at higher Q^2 the values of δ reach those expected from a hard process.

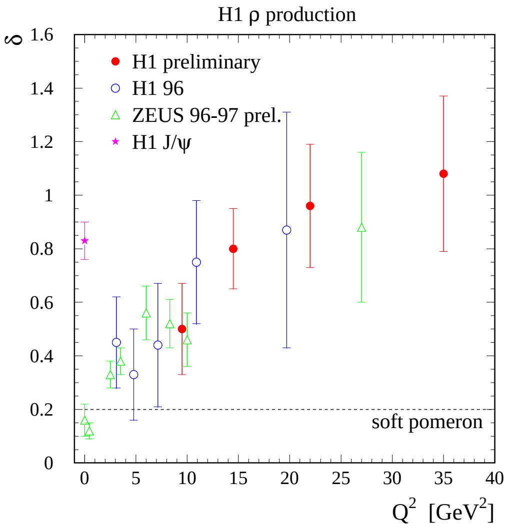

Fig. 11. The parameter δ from a fit of the form W^δ to the cross section data of ρ^0 electroproduction, as function of Q^2.

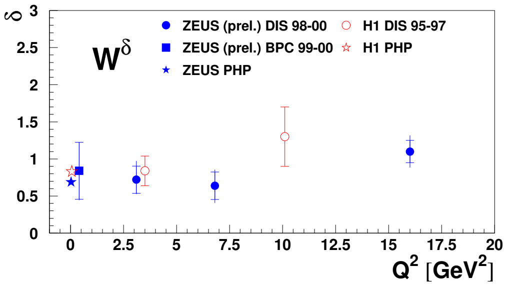

Fig. 12. The parameter δ from a fit of the form W^δ to the cross section data of J/ψ electroproduction, as function of Q^2.

However, in case of exclusive electroproduction of J/ψ [20,21], the hard scale is provided by the heavy quark mass and thus the value of δ is already large even at $Q^2 = 0$, as shown in Fig. 12.

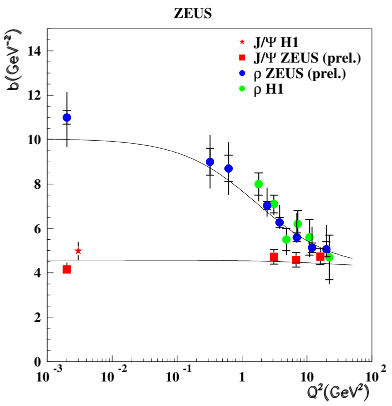

Fig. 13. The slope b of $d\sigma/dt$ for ρ^0 and J/ψ.

Another way of seeing this different behavior of the light and heavy vector mesons, is through the study of the Q^2 dependence of the slope b of the differential cross section $d\sigma/dt$ of ρ^0 and J/ψ. Fig. 13 displays the measured value of b as function of Q^2, for both vector mesons. One sees the clear soft-hard transition in case of the ρ^0, while the J/ψ production is a hard process even in case of photoproduction. At $Q^2 \geq 20$ GeV^2, both mesons have the same small size, and the b value is as expected from the proton size [22].

Contrary to the photoproduction case, in the electroproduction of vector mesons both transversely and linearly polarized photons participate. In the picture discussed above, where the photon fluctuates into a quark-antiquark dipole, it can do so in two configurations: a large spatial one, resulting in a soft process, and a small spatial one, resulting in a hard process [23]. While the longitudinal photon is believed to fluctuate into a small configuration, the transverse photon can fluctuate into both. It is of interest to study how the different configurations of the virtual photon influence the soft-hard transition discussed above. To this end, one can use s-channel helicity conservation to measure the ratio $R = \sigma_L/\sigma_T$ of the cross sections produced by longitudinal to transverse photons.

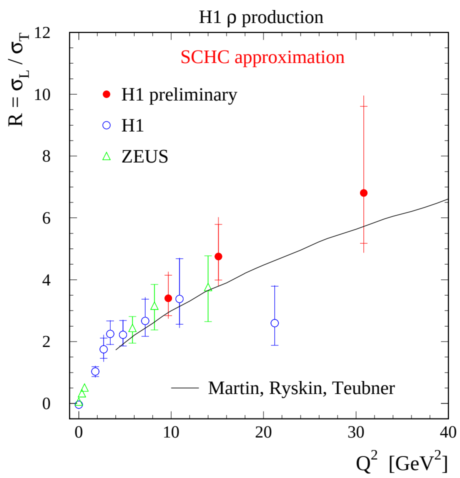

Fig. 14. The ratio R as function of Q^2 for ρ^0 electroproduction. The curve is the expectation of the MRT model [26].

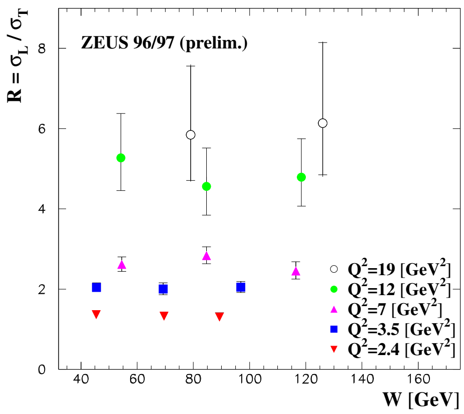

Fig. 15. The W dependence of R for ρ^0 electroproduction, for fixed Q^2 bins.

Fig. 14 shows the ratio R for electroproduction of ρ^0, as function of Q^2 [18,25]. The cross section coming from the longitudinal photon dominates as Q^2 gets larger, and this increase is well described by the MRT model [26]. What is surprising is the fact that R seems to be independent of W, in the Q^2 range where the measurements were performed, as shown in Fig. 15 [18]. This means that the W dependence of σ_T is the same as σ_L, from which one concludes that the large size configuration of the transverse photons is suppressed for ρ^0 electroproduction. The statistics of the J/ψ electroproduction data do not allow at present to check whether this striking feature holds also for the heavy VM case.

Another striking results in case of the electroproduction of ρ^0 is shown in Fig. 16, where the ratio of the electroproduction to the total $\gamma^* p$ cross sections is displayed. This ratio is W independent over the whole measured kinematic region [27]. This is contrary to expectations of both the Regge approach as well as the pQCD one. In case of the J/ψ, the ratio increases with W, and the increase is consistent with expectations from both approaches.

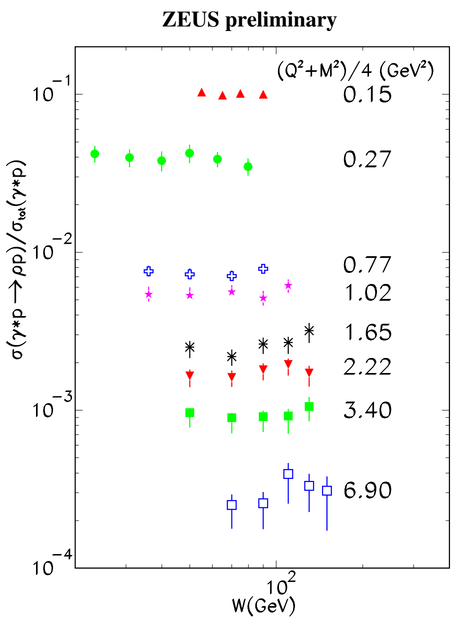

Fig. 16. The ratio of the ρ^0 electroproduction cross section to the total $\gamma^* p$ one, as function of W, at different scales.

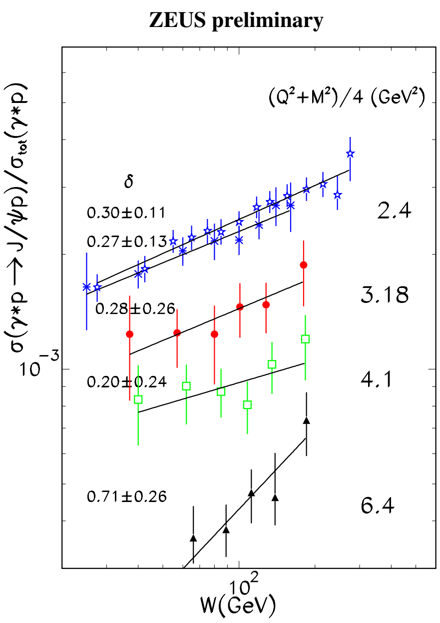

Fig. 17. The ratio of the J/ψ electroproduction cross section to the total $\gamma^* p$ one, as function of W, at different scales. The lines are a best fit of the form W^{δ} to the data.

6 Deeply Virtual Compton Scattering (DVCS)

Deeply virtual Compton scattering (DVCS) is a similar process to electroproduction of VMs, where the final state vector is replaced by a real photon. The DVCS initial and final states are identical to those of the QED Compton process. The diagrams of both processes are shown in Fig. 18.

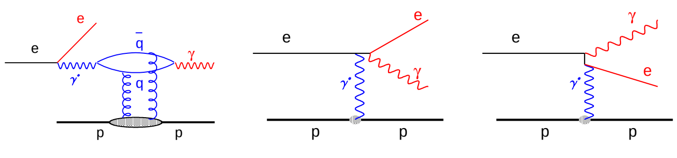

Fig. 18. Diagrams showing the QCD DVCS process and the QED Compton process.

The big interest in DVCS comes from the fact that the QED and QCD amplitudes interfere and produces an asymmetry which can be measured, once high statistics data are at hand. This would give information on the real part of the QCD amplitude. In addition, the DVCS process is a potential one for obtaining generalized parton distributions [28].

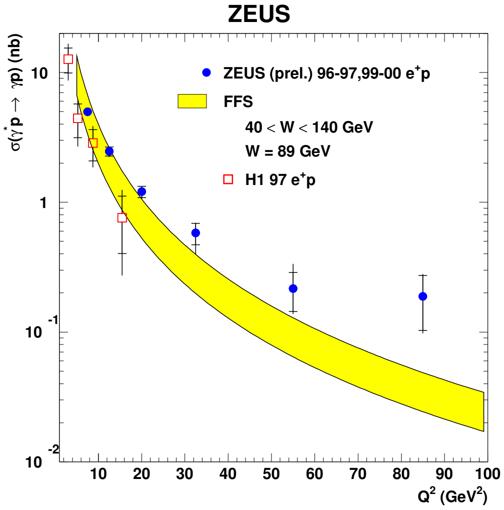

Fig. 19. The DVCS cross section as function of Q^2. The band is a theoretical prediction [31].

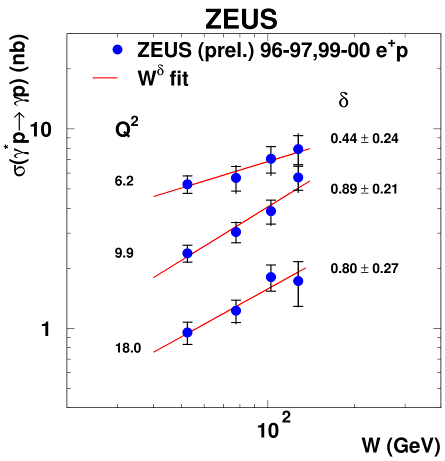

Fig. 20. The DVCS cross section as a function of W for fixed Q^2 values. The line is a fit of the form W^δ to the data.

The Q^2 dependence of the DVCS cross section is shown in Fig. 19 [29,30]. Its fall-off with Q^2 is well described by the Frankfurt, Freund and Strikman model [31]. The W dependence of the DVCS cross section is shown in Fig. 20 [29], for fixed Q^2 values. Fitting the data to a form of W^δ shows that the cross section rises steeply as Q^2 increases. It reaches the same value of δ as in the hard process of J/ψ electroproduction. Given the fact that the final state photon is real, and thus transversely polarized, the DVCS process is produced by transversely polarized virtual photons, assuming s-channel helicity. The steep energy dependence thus indicates that the large configurations of the virtual transverse photon are suppressed. This is the same conclusion as we obtained above in the case of the electroproduction of ρ^0.

Acknowledgments

I would like to thank the organizers for a very pleasant conference. I would also like to acknowledge the partial support of the Israel Science Foundation (ISF) and the German Israel Foundation (GIF), which made this contribution possible.

References

1. P. D. Collins, "An Introduction to Regge Theory and High-Energy Physics", Cambridge University Press, 1977.
2. V. N. Gribov, JEPT Lett. **41** (1961) 667.
3. A. Donnachie and P. V. Landshoff, Phys. Lett. **B296** (1992) 227.
4. F. E. Low, Phys. Rev. **D12** (1975) 163; S. Nussinov, Phys. Rev. Lett. **34** (1975) 1286.
5. See e.g. H. Abramowicz, Nucl. Phys. **B** (Proc. Suppl.) **99** (2001) 79, and references therein.
6. J. C. Collins, Phys. Rev. **D57** (1998) 3051; erratum Phys. Rev. **D61** (1998) 2000.
7. A. Berera and D. E. Soper, Phys. Rev. **D53** (1996) 6162.
8. L. Trentadue and G. Veneziano, Phys. Lett. **B323** (1994) 201.
9. G. Ingelman and P. E. Schlein, Phys. Lett. **B152** (1985) 256.
10. ZEUS Collab., paper #823 submitted to ICHEP02, Amsterdam 2002.
11. H1 Collab., paper #980 submitted to ICHEP02, Amsterdam, 2002.
12. H. Abramowicz and A. Levy, DESY 97-251 (1997).
13. H1 Collab., paper #987 submitted to ICHEP02, Amsterdam, 2002.
14. ZEUS Collab., paper #832 submitted to ICHEP02, Amsterdam 2002.
15. L. Frankfurt and M. Strikman, hep-ph/9907221, (1999).
16. ZEUS Collab., paper #821 submitted to ICHEP02, Amsterdam 2002.
17. S. J. Brodsky et al., Phys. Rev. **D50** (1994) 3134.
18. A. Kreisel for the ZEUS Collab., Proceedings of DIS01, Bologna, 2001.
19. H1 Collab., paper # 989 submitted to ICHEP02, Amsterdam, 2002.
20. ZEUS Collab., paper #813 submitted to ICHEP02, Amsterdam, 2002.
21. H1 Collab., C.Adloff et al., Eur. Phys. J **C10** (1999) 373.
22. H. Abramowicz, L. Frankfurt and M. Strikman, Surveys High Energy Phys. **11** (1997) 51.
23. J. Bjorken, AIP Conference Proceedings No. 6, Particles and Fields Subseries No. 2, ed. M. Bander, G. Shaw and D. Wong (AIP, New York, 1972).
24. ZEUS Collab., paper #818 submitted to ICHEP02, Amsterdam 2002.
25. H1 Collab., paper #989 submitted to ICHEP02, Amsterdam 2002.
26. A. D. Martin, M. G. Ryskin and T. Teubner, Phys. Rev. **D55** (1997) 4329; Phys. Rev. **D56** (1997) 3007.
27. ZEUS Collab., paper #820 submitted to ICHEP02, Amsterdam 2002.
28. See e.g. A. V. Radyushkin, Phys. Rev. **D58** (1998) 114008.
29. ZEUS Collab., paper # 825 submitted to ICHEP02, Amsterdam, 2002.
30. H1 Collab., C. Adloff et al., Phys. Lett. **B517** (2001) 47.
31. L. Frankfurt, A. Freund and M. Strikman, Phys. Rev. **D58** (1998) 114001; erratum Phys. Rev. **D59** (1999) 119901.